

LOFAR DISCOVERY OF A RADIO HALO IN THE HIGH-REDSHIFT GALAXY CLUSTER PSZ2 G099.86+58.45

R. CASSANO¹, A. BOTTEON^{1,2,3}, G. DI GENNARO³, G. BRUNETTI¹, M. SERENO^{4,5}, T.W. SHIMWELL^{6,3}, R.J. VAN WEEREN³, M. BRÜGGEN⁷, F. GASTALDELLO⁸, L. IZZO⁹, L. BÎRZAN⁷, A. BONAFEDE^{2,7}, V. CUCITI⁷, F. DE GASPERIN⁷, H.J.A. RÖTTGERING³, M. HARDCASTLE¹⁰, A.P. MECHEV³, C. TASSE^{11,12}

¹INAF - Istituto di Radioastronomia, via P. Gobetti 101, I-40129 Bologna, Italy

²Dipartimento di Fisica e Astronomia, Università di Bologna, via P. Gobetti 93/2, I-40129 Bologna, Italy

³Leiden Observatory, Leiden University, P.O. Box 9513, 2300 RA Leiden, The Netherlands

⁴INAF - Osservatorio di Astrofisica e Scienza dello Spazio, via P. Gobetti 93/3, I-40129 Bologna, Italy

⁵INFN, Sezione di Bologna, viale Berti Pichat 6/2, 40127 Bologna, Italy

⁶ASTRON - Netherlands Institute for Radio Astronomy, PO Box 2, 7990 AA Dwingeloo, The Netherlands

⁷Universität Hamburg, Hamburger Sternwarte, Gojenbergsweg 112, 21029, Hamburg, Germany

⁸INAF/IASF - Milano, Via A. Corti 12, I-20133 Milan, Italy

⁹Instituto de Astrofísica de Andalucía (IAA-CSIC), Glorieta de la Astronomía s/n, E-18008, Granada, Spain

¹⁰Centre for Astrophysics Research, School of Physics, Astronomy and Mathematics, University of Hertfordshire, College Lane, Hatfield AL10 9AB, UK

¹¹GEPI, Observatoire de Paris, Université PSL, CNRS, 5 Place Jules Janssen, 92190, Meudon, France and

¹²Department of Physics & Electronics, Rhodes University, PO Box 94, Grahamstown, 6140, South Africa

Draft version July 25, 2019

ABSTRACT

In this Letter, we report the discovery of a radio halo in the high-redshift galaxy cluster PSZ2 G099.86+58.45 ($z = 0.616$) with the LOw Frequency ARray (LOFAR) at 120-168 MHz. This is one of the most distant radio halos discovered so far. The diffuse emission extends over ~ 1 Mpc and has a morphology similar to that of the X-ray emission as revealed by *XMM-Newton* data. The halo is very faint at higher frequencies and is barely detected by follow-up 1-2 GHz Karl G. Jansky Very Large Array (JVLA) observations, which enable us to constrain the radio spectral index to be $\alpha \lesssim 1.5 - 1.6$, *i.e.*, with properties between canonical and ultra-steep spectrum radio halos. Radio halos are currently explained as synchrotron radiation from relativistic electrons that are re-accelerated in the intra-cluster medium (ICM) by turbulence driven by energetic mergers. We show that in such a framework radio halos are expected to be relatively common at ~ 150 MHz ($\sim 30 - 60\%$) in clusters with mass and redshift similar to PSZ2 G099.86+58.45; however, at least 2/3 of these radio halos should have steep spectrum and thus be very faint above ~ 1 GHz frequencies. Furthermore, since the luminosity of radio halos at high redshift depends strongly on the magnetic field strength in the hosting clusters, future LOFAR observations will also provide vital information on the origin and amplification of magnetic fields in galaxy clusters.

Subject headings: Galaxies: clusters: individual (PSZ2 G099.86+58.45) — Galaxies: clusters: intracluster medium — large-scale structure of universe — Radiation mechanisms: non-thermal — X-rays: galaxies: clusters

1. INTRODUCTION

Cluster-scale (\sim Mpc-scale), diffuse synchrotron emission is frequently found in high-mass ($M_{500} \gtrsim 5 \times 10^{14} M_{\odot}$) merging galaxy clusters in the form of so-called giant radio halos (hereafter RHs), apparently unpolarised emission that fills large cluster volumes (*e.g.*, van Weeren et al. 2019). These sources are characterised by low surface brightnesses and steep spectra ($\alpha > 1$, with $S_{\nu} \propto \nu^{-\alpha}$, this is the convention we adopt in this paper). Their properties and connection with clusters mergers support the idea that they trace turbulent regions in the intra-cluster medium (ICM) where relativistic particles are trapped and re-accelerated during cluster-cluster mergers (*e.g.*, Brunetti & Jones 2014).

Present statistical studies are limited to relatively low-redshift systems ($z \lesssim 0.35 - 0.4$; *e.g.*, Venturi et al. 2007, 2008; Kale et al. 2015; Cuciti et al. 2015), with only a handful of halos discovered at $z \simeq 0.5 - 0.6$ (Giovannini

& Feretti 2000; Bonafede et al. 2009, 2012; van Weeren et al. 2009) and only two at higher redshift, one located in the *El Gordo* galaxy cluster, an exceptionally massive object at $z = 0.87$ (Lindner et al. 2014) and one in PLCKG147.32–16.59, a cluster at $z = 0.65$ (van Weeren et al. 2014). At high redshift an increasing fraction of the energy that is dumped into the acceleration of relativistic electrons in RHs is radiated away in the form of inverse Compton (IC) emission, $dE/dt \propto (1+z)^4$. This is expected to cause a decline of the fraction of RHs in high- z galaxy clusters with respect to their low- z counterparts (Cassano et al. 2006). In particular the fraction of clusters hosting RHs at higher z is also expected to be very sensitive to the magnetic fields in these systems.

The discovery of high-redshift RHs has been limited by the need for radio observations with high sensitivity to steep spectrum emission and high resolution to adequately distinguish the emission from contaminating sources. The advent of the LOw Frequency ARray (LOFAR; van Haarlem et al. 2013), which can produce

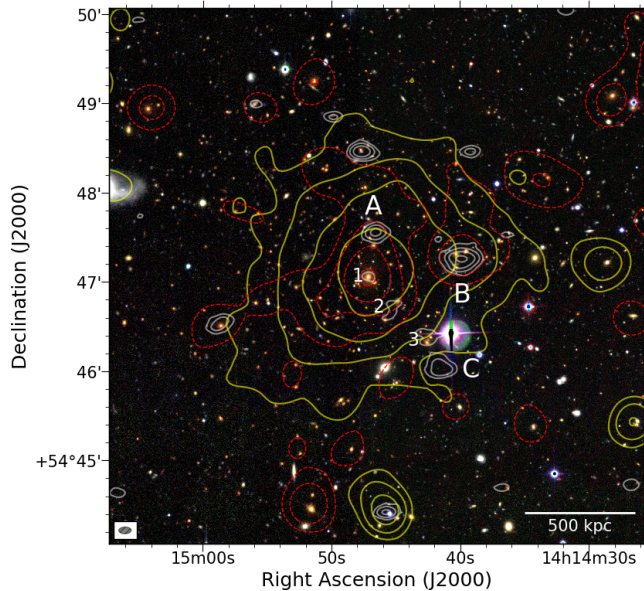


FIG. 1.— CFHTLenS g , r and i band composite images of PSZ2G099 with overlaid the LOFAR 144 MHz high resolution ($8.3'' \times 4.3''$) contours (white), the *XMM-Newton* contours (yellow) and light density contours of the cluster member galaxies (red-dashed). Contours are spaced by a factor of 3 starting from 5σ for LOFAR (where $\sigma = 70 \mu\text{Jy beam}^{-1}$) and by a factor of 2 starting from $5.0 \times 10^{-6} \text{ counts s}^{-1} \text{ pixel}^{-1}$ for *XMM-Newton* (cf. Fig. 2, center). The LOFAR beam is shown in the lower left corner. Labels and numbers show the position of the radio sources (see Sect.3 for details).

deep, high-resolution, high-fidelity, low-frequency radio images, has opened up the possibility to study RHs at low frequencies with unprecedented detail and sensitivity (*e.g.*, van Weeren et al. 2016a; Shimwell et al. 2016; Bonafede et al. 2018; Botteon et al. 2018, 2019; Hoang et al. 2018, 2019a,b; Wilber et al. 2018, 2019).

In this Letter, we report on the discovery of a radio halo in the high-redshift galaxy cluster PSZ2 G099.86+58.45 (PSZ2G099, hereafter) which was observed as part of the LOFAR Two-metre Sky Survey (LoTSS). LoTSS is an ongoing sensitive $\sim 100 \mu\text{Jy}/\text{beam}$, high-resolution, $\sim 6''$, 120-168 MHz survey of the entire northern sky (Shimwell et al. 2017, 2019).

PSZ2G099 is a massive, $M_{500} = (6.84 \pm 0.48) \times 10^{14} M_{\odot}$ (Planck Collaboration et al. 2016) and hot, $kT = 8.9_{-1.1}^{+2.8}$ keV (Serenio et al. 2018) cluster discovered through its Sunyaev-Zel'dovich (SZ) signal by the *Planck* satellite. Recently, the gravitational lensing signal of this cluster has been traced up to 30 Mpc from its centre implying that it sits in a very high-density environment, about six times denser than the average ΛCDM prediction at this redshift (Serenio et al. 2018). The expected complex dynamics around this cluster make the discovery of a RH in this cluster particularly interesting.

Hereafter, we adopt a ΛCDM cosmology with $H_0 = 70 \text{ km s}^{-1} \text{ Mpc}^{-1}$, $\Omega_m = 0.3$, and $\Omega_{\Lambda} = 0.7$. With the adopted cosmology, $1''$ corresponds to a length scale of 6.766 kpc at $z = 0.616$.

2. OBSERVATIONS & DATA REDUCTION

The LoTSS pointings consist of 8 hr observations in the 120 – 168 MHz band, which are typically separated

by $\sim 2.6^\circ$. PSZ2G099 is located at $\sim 15'$ from the center of pointing P214 + 55 (in the region of the HETDEX Spring Field), acquired on 14 May 2015 (ObsID L343224). Data reduction of this pointing was performed with the pipeline described by Shimwell et al. (2019), which performs direction-independent and dependent calibration and imaging of the full LOFAR field-of-view, using PREFACTOR (van Weeren et al. 2016b; Williams et al. 2016; de Gasperin et al. 2019; Mechev et al. 2018), KILLMS (Tasse 2014a,b; Smirnov & Tasse 2015) and DDFACET (Tasse et al. 2018). To improve the image quality in the direction of PSZ2G099, we used the products of the pipeline, subtracted all the sources outside a region of $15' \times 15'$ surrounding the target, and performed extra phase and amplitude self-calibration loops in this sub-field (more details by van Weeren et al. in prep.). The LOFAR images shown in this paper were produced with WSClean v2.6 (Offringa et al. 2014) and have a central frequency of 144 MHz. Uncertainties on the LOFAR integrated flux densities are dominated by errors in the absolute flux scale, which is conservatively set to 20%, in line with LoTSS measurements (Shimwell et al. 2019).

A follow-up observation of PSZ2G099 was carried-out with the Karl G. Jansky Very Large Array (JVLA) in the L-band (*i.e.*, 1–2 GHz) in C- and D-configurations, for a total time of 4 hrs. Following the procedure described by Di Gennaro et al. (2018), we calibrated the antenna delays, bandpass, cross-hand delays, and polarisation leakage and angles using the primary calibrators 3C286 and 3C147. The calibration solutions were then applied to the target, and self-calibration on the single dataset was performed to refine its amplitude and phase solutions. During the final self-calibration on the combined dataset we also employed an additional self-calibration on a bright source located at the edge of the primary beam, whose side lobes affect the cluster radio emission. All the images in this paper were produced with CASA v5.0 (McMullin et al. 2007) using w-projection (Cornwell et al. 2005, 2008), Briggs weighting with `robust=0`, `nterms=3` (Rau & Cornwell 2011) and are corrected for the primary beam attenuation.

PSZ2G099 was observed three times with *XMM-Newton* (ObsID: 0693660601, 0693662701, 0723780301) for a total exposure time of 63 ks. Periods of the observations that were affected by soft proton flares are excluded during the analysis by using the Scientific Analysis System tasks. The displayed image is a background-subtracted and exposure-corrected mosaic image in the 0.5 – 2.0 keV band of the three ObsIDs where MOS and pn camera images are combined.

3. RESULTS

A multi-wavelength view of PSZ2G099 is reported in Fig. 1 where the LOFAR high-resolution contours are overlaid on the CFHTLenS (Canada France Hawaii Telescope Lensing Survey, Heymans et al. 2012) image highlighting the presence of the compact radio sources in the direction of the cluster. The X-ray contours from *XMM-Newton* are also reported to show the distribution of the thermal gas. The red contours follow the average surface density of the cluster member galaxies selected in the optical i -band. We select 3058 galaxies from the CFHTLenS image with photometric redshift

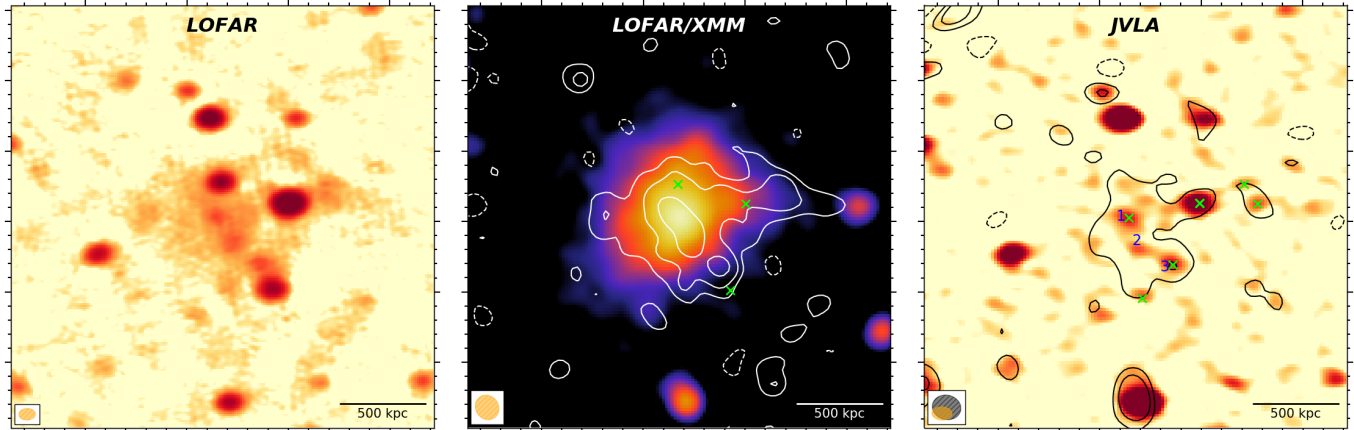


FIG. 2.— Left: LOFAR 144 MHz medium-resolution ($13.9'' \times 9.7''$, rms noise $\sigma = 90 \mu\text{Jy beam}^{-1}$). Center: *XMM-Newton* image in the 0.5 – 2.0 keV band smoothed with a 3-pixel Gaussian kernel (1 pixel = $2.5''$) with low-resolution source-subtracted LOFAR contours ($21.6'' \times 19.4''$, $\sigma = 200 \mu\text{Jy beam}^{-1}$) spaced by a factor of 2 starting from 2σ . In both panels, -2σ contours are displayed in dashed lines while the beam shapes are shown in the bottom left corners. Right: 1–2 GHz high-resolution ($17.1'' \times 11.2''$, $\sigma = 20 \mu\text{Jy beam}^{-1}$) JVLA image with 2.5σ and 5σ low-resolution source-subtracted JVLA contours ($24.5'' \times 20.8''$, $\sigma = 36 \mu\text{Jy beam}^{-1}$). Numbers in the right panel show the position of the three blobs also highlighted in Fig. 1.

TABLE 1
RADIO HALO PROPERTIES

$S_{\text{halo}, 144 \text{ MHz}}$ (mJy) ^a	25.3 ± 5.7
$S_{\text{halo}, 1500 \text{ MHz}}$ (mJy)	$\sim 1.5 \pm 0.5$
$F_{\text{halo}, 1.4 \text{ GHz}}$ ($10^{24} \text{ W Hz}^{-1}$) ^b	2.85 ± 0.95
Halo Size (Mpc)	0.6–1.2
144 MHz compact source fluxes (mJy)	7.0 ± 1.4 (A)
	30.9 ± 6.2 (B)
	7.4 ± 1.5 (C)

^a integrated (within $2\sigma_{\text{rms}}$) RH flux density.

^b assuming a spectral index of $\alpha = 1.2$ for the halo emission, k -corrected.

within $\pm 0.06(1 + z_{\text{cl}})$ of the cluster redshift, comparable to the survey photo- z uncertainty. The distribution was smoothed with a Gaussian kernel with a standard deviation of $50 \text{ kpc}/h$. The double-peaked average surface density and the elongated X-ray emission indicate that PSZ2G099 is in a merging phase.

At medium resolution (Fig. 2, left panel), LOFAR clearly reveals extended diffuse emission at the center of the galaxy cluster. Subtracting the emission from point sources and tapering down to $\sim 20''$ resolution (central panel) we find a total extent of $\sim 3 \times 1.5'$ in the east-west and north-south direction, respectively, corresponding to a physical extent of $\sim 1.2 \times 0.6 \text{ Mpc}$. We classify this emission as a RH due to its extension, morphology, and location in the cluster. The integrated flux density of the sources labelled A, B, and C located in the RH region (Fig. 1) is reported in Tab. 1. Among these only source B is detected in the JVLA image and has a spectral index $\alpha \simeq 1.5$ (see Fig. 2, right panel), meaning that source A and C are very steep spectrum sources ($\alpha > 1.8$). In the high-resolution LOFAR image, another three blobs of emission are detected at 5σ (numbered from 1 to 3 in Fig. 1) which account for a small total flux density of $S_{144 \text{ MHz}} \sim 3 \text{ mJy}$. These are also detected at high-frequency, as seen in Fig. 2 (right panel).

To disentangle the contribution of the point sources and provide a reliable measurement of the RH flux den-

sity we create an image of diffuse emission only (Fig. 2, central panel) by subtracting the clean components of the sources A, B and C from the visibilities obtained by applying an inner uv -cut of $3.5 \text{ k}\lambda$ (corresponding to a linear size of about 400 kpc at $z = 0.616$) to the data. The flux density of the halo measured within the LOFAR 2σ contour is $S_{144 \text{ MHz}} = 25.3 \pm 5.7 \text{ mJy}$ (this excludes the 3 mJy flux of the three blobs). We verified that the subtraction of the three point sources using uv -cuts in the range $2.0 - 5.5 \text{ k}\lambda$ (corresponding to scales of $\sim 700 - 250 \text{ kpc}$ at the cluster redshift) corresponds to variations of the RH flux density of $\sim 27.2 - 31.6 \text{ mJy}$, which is within the calibration error. The diffuse flux density is $\sim 15\%$ lower if emission above the 3σ level is considered.

In Fig. 2 (right panel) we show the JVLA high-resolution ($17.1'' \times 11.2''$) image with the 2.5σ contours from the JVLA low-resolution source-subtracted image. The latter image has been obtained after the subtraction of the clean components of the point sources in the field (including those outside the cluster region) using an uv -cut of $1.3 \text{ k}\lambda$ (corresponding to $\sim 500 \text{ kpc}$) and `robust=-0.5`, and then tapering at $\sim 20''$ resolution. The rms noise of this map is $36 \mu\text{Jy}/\text{beam}$. Diffuse emission from the RH region is barely detected (the halo is not clearly detected at 3σ) but shows some similarity with the RH seen by LOFAR. However, the JVLA image appears to be contaminated by residuals of radio emission by individual sources. Indeed, from the un-tapered map in which point sources have been subtracted, we estimate that a residual contribution of $\sim 1 \text{ mJy}$ can still be attributed to point sources which leads to a residual RH flux density of 1.5 mJy within 2σ . Because of the very low brightness of the halo we evaluated the statistics of the diffuse flux extracted from similar regions around the RH measuring residual flux densities which range between $\approx -0.3 \text{ mJy}$ and $+0.6 \text{ mJy}$. This provides an uncertainty in the determination of the RH flux of $\approx \pm 0.5 \text{ mJy}$ at 1.5 GHz .

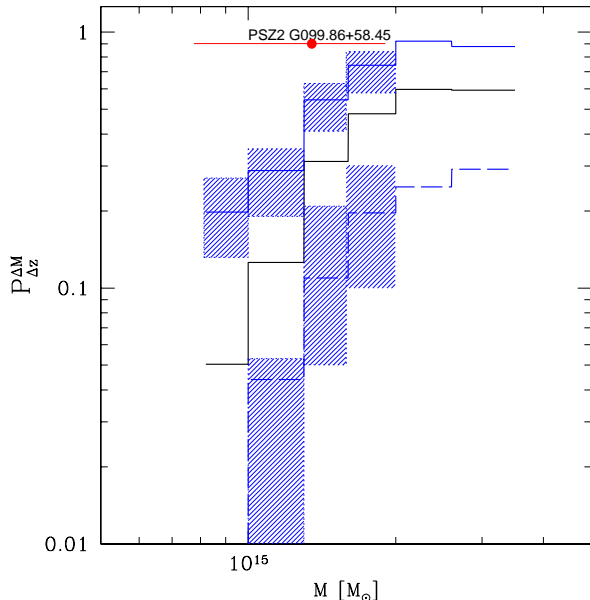


FIG. 3.— Probability to form RHs with $\nu_s \gtrsim 120$ MHz (solid curves) and with $\nu_s \gtrsim 1400$ MHz (dashed curves) as a function of the cluster virial mass in the redshift range 0.6–0.7, for $B = 1 \mu\text{G}$ (black curve) and $B = 4.8 \mu\text{G}$ (blue line). For the latter case, the 1σ uncertainty derived through Monte Carlo calculations is also shown (blue shadowed regions, see text).

4. DISCUSSION

Observing high- z RHs provides unique information on the physics of these sources in an extreme environment. In fact, models for the origin of RHs at such early times are challenged by the strong IC-losses of relativistic electrons ($dE/dt \propto E^2(1+z)^4$) which would compete and hamper the acceleration of high-energy electrons and reduce the synchrotron luminosity that is generated by a factor B^2/B_{cmb}^2 . Under these conditions the maximum synchrotron frequency emitted by the electrons accelerated in RHs depends on B/B_{cmb}^2 (Cassano et al. 2006) and thus the magnetic field sets the frequency window where the emission can be observed.

To investigate this point, we derive the formation probability of RHs in a cluster with mass and redshift similar to PSZ2G099 using the statistical model developed by (Cassano & Brunetti 2005, see also Cassano et al. 2006, 2010) which is based on the turbulent re-acceleration scenario. These models match the observed fraction of clusters with RHs derived in mass-selected cluster sample at low- z (Cuciti et al. 2015). In such a framework, the synchrotron spectra of RHs steepen at high frequencies since turbulent re-acceleration is balanced by radiative losses of relativistic electrons. This steepening makes it difficult to detect RHs at frequencies higher than the frequency ν_s at which the steepening becomes severe^a. As a simplified approach to estimate the occurrence of RHs at a given frequency ν_0 we assume that only halos with $\nu_s > \nu_0$ can be observed at ν_0 . Massive, merging clusters should statistically have larger values of ν_s making them detectable at relatively high frequencies (\sim GHz),

^a ν_s is defined as the frequency where the synchrotron spectrum is $\alpha = 1.9$, with α calculated between $\nu_s/2.5$ and ν_s (see Cassano et al. 2010, for details)

while less energetic mergers are expected to produce RHs with lower ν_s which are only detectable at low frequencies ($<$ few 100 MHz). The latter are referred to as ultra-steep spectrum RHs (USSRHs^b) and are predicted to be the dominant class of RHs in low-frequency radio surveys, such as LoTSS (Brunetti et al. 2008; Cassano et al. 2010; Wilber et al. 2018). Theoretically, the two classes of RHs, the canonical and USSRHs, mark the extremes of a continuous distribution of properties of these radio sources.

In Fig. 3, we show the probability to form RHs with $\nu_s \gtrsim 120$ MHz (solid curves) and with $\nu_s \gtrsim 1400$ MHz (dashed curves) for clusters in the redshift range 0.6–0.7. We assume two values for the average magnetic field strength in the RH region: $\sim 1 \mu\text{G}$ (black line) and $B = 4.8 \mu\text{G}$ (blue line). The latter value corresponds to the magnetic field that maximises the lifetime of relativistic electrons radiating at a given observing frequency at the redshift of the system (*i.e.*, $B \simeq B_{cmb}/\sqrt{3} \simeq 4.8 \mu\text{G}$), and thus it should be considered an upper limit for the model expectations. For the case $B = 4.8 \mu\text{G}$, we also report the resulting probabilities derived by 1000 Monte Carlo extractions of galaxy cluster samples from the pool of simulated merger trees (shadowed blue regions). Considering the virial mass of PSZ2G099, $M_v \simeq (1.35 \pm 0.57) \times 10^{15} M_{\odot}$ (Serenio et al. 2017), we find that at low frequency the probability to form a RH in such a cluster is maximum 40 to 60%, while it drops to about 30% considering $B \sim 1 \mu\text{G}$. We conclude that RHs in clusters similar to PSZ2G099 should be fairly common in LOFAR surveys. On the other hand, the probability to form RHs in these systems at high frequencies ($\nu_s \simeq 1400$ MHz) is found to depend critically on the magnetic field in the emitting volume. The maximum probability ($B = 4.8 \mu\text{G}$) is about 20% whereas a very small probability (below the percent level, not visible in Fig. 3) is obtained considering $B = 1 \mu\text{G}$. The drop in probability between low and high frequencies is essentially due to the presence of USSRHs that glows up preferentially at lower frequencies.

For the specific case of PSZ2G099 the spectrum is not measured well, however our constraint $\alpha \lesssim 1.5 - 1.6$ implies that we can exclude the case of a RH with an extremely steep spectrum, and that the radio properties of PSZ2G099 could be intermediate between those of canonical and USSRHs. We measure a RH flux density at 1.5 GHz of $\sim 1.5 \pm 0.5$ mJy, implying a 1.4 GHz radio power (k -corrected) $P_{1.4} \simeq (2.85 \pm 0.95) \times 10^{24} \text{ W Hz}^{-1}$, which is consistent with the $P_{1.4} - M_{500}$ correlation observed in intermediate redshift clusters (Cassano et al. 2013). This provides information on the magnetic field in the RH volume. The expected radio luminosity is $P_{syn} \propto \eta_{rel}(\rho v_t^3/L_{inj})/(1 + (B_{cmb}/B)^2)$ (where η_{rel} account for the fraction of turbulence dissipated in particle acceleration). Although the turbulent dissipation rate ($\rho v_t^3/L_{inj}$, with ρ gas density, v_t turbulent velocity and L_{inj} the turbulence injection scale) can be larger in dynamically-young high- z clusters than in low- z ones, the fact that the radio power of PSZ2G099 is similar to its lower- z counterparts suggests that B in this cluster is

^b RHs with $\alpha > 1.5$ are considered USSRHs (see discussion in Brunetti 2004; Brunetti et al. 2008)

at least similar to that in low- z ones.

This finding provides important information for models of amplification of B in galaxy clusters, in particular on the origin of the seed field that is stirred and amplified by turbulence and small scale dynamo (Dolag et al. 2005; Vazza et al. 2018; Donnert et al. 2018). Since the dynamo mechanism is a slow process that requires several turbulent eddy-turnover times (several Gyrs, *e.g.*, Vazza et al. 2018, and ref. therein) our observations suggest an important role of Active Galactic Nuclei (AGN) and Galactic Winds (GW) in setting a significant seed field in the ICM at high redshift.

At the same time it should be stressed that PSZ2G099 is sitting in a special region of the Universe, which was found to be about six times denser than the average density of the Universe at that redshift (Sereni et al. 2018); its RH could therefore be unique. The effect of the large-scale environment (environment-bias; see Mao et al. 2018, and ref. therein) can trigger the formation of a RH: in such a place more merger/accretion episodes are expected to *bias* the halo growth with respect to cluster of similar mass in less denser regions of the Universe. As a consequence, future analysis of LOFAR surveys will be very important to constrain the formation rate of RHs at high- z and the origin of magnetic fields in these systems.

5. CONCLUSIONS

We report on the discovery of a \sim Mpc (total extent) RH in the PSZ2G099 cluster using LOFAR observations at 120 – 168 MHz carried out for the LoTSS. Being at a redshift of \sim 0.616 it is among the most distant RHs discovered so far, and the furthest away currently discovered by LOFAR.

The halo is also barely detected by 1-2 GHz follow-up JVLA observations that constrains the radio spectral index to be $\alpha \lesssim 1.5 - 1.6$, *i.e.*, with properties between canonical and ultra-steep spectrum radio halos. The estimated 1.4 GHz radio power locates the halo on the observed $P_{1.4} - M_{500}$ correlation meaning that the magnetic field strength in this cluster should be not much different from that of other low to intermediate redshift halos in clusters with similar mass.

We show that current turbulent reacceleration models predict that RHs in clusters similar to PSZ2G099 should be common (\sim 30 – 60%) at low frequencies, however at least 2/3 of these RHs should be USSRHs and thus be very faint at high-frequencies. This shows the power of LOFAR as a unique machine to discover RHs at high- z .

Furthermore, since the fraction of clusters with RHs (and with USSRHs) at high- z and their luminosity depend on the magnetic field in these systems we claim that LOFAR statistical studies of high- z RHs will provide vital information on the origin of magnetic fields in galaxy clusters.

Acknowledgments: This paper is based on data obtained from the International LOFAR Telescope (ILT) under project code LC3.008. LOFAR (van Haarlem et al. 2013) is the Low Frequency Array designed and constructed by ASTRON. It has observing, data processing, and data storage facilities in several countries, which are owned by various parties (each with their own funding sources), and are collectively operated by the ILT foundation under a joint scientific policy. The ILT resources have benefitted from the following recent major funding sources: CNRS-INSU, Observatoire de Paris and Université d’Orléans, France; BMBF, MIWF-NRW, MPG, Germany; Science Foundation Ireland (SFI), Department of Business, Enterprise and Innovation (DBEI), Ireland; NWO, The Netherlands; The Science and Technology Facilities Council, UK; Ministry of Science and Higher Education, Poland; Istituto Nazionale di Astrofisica (INAF), Italy. This research made use of the Dutch national e-infrastructure with support of the SURF Cooperative (e-infra 180169) and the LOFAR e-infra group. The Jülich LOFAR Long Term Archive and the German LOFAR network are both coordinated and operated by the Jülich Supercomputing Centre (JSC), and computing resources on the Supercomputer JUWELS at JSC were provided by the Gauss Centre for Supercomputing e.V. (grant CHTB00) through the John von Neumann Institute for Computing (NIC). This research made use of the University of Hertfordshire high-performance computing facility and the LOFAR-UK computing facility located at the University of Hertfordshire and supported by STFC [ST/P000096/1], and of the LOFAR IT computing infrastructure supported and operated by INAF, and by the Physics Dept. of Turin University (under the agreement with Consorzio Interuniversitario per la Fisica Spaziale) at the C3S Supercomputing Centre, Italy. M.S. acknowledges financial contribution from ASI-INAF n.2017-14-H.0. The Leiden LOFAR team acknowledge support from the European Research Council under the FP/2007-2013/ERC Advanced Grant NEWCLUSTERS-321271. RJvW acknowledges support from the VIDJ research programme, project number 639.042.729, which is financed by the NWO. ABon acknowledges financial support from the ERC-Stg DRANOEL, no 714245, and from the MIUR grant FARE SMS. L.I. acknowledges support from funding associated with Juan de la Cierva Incorporacion fellowship IJCI-2016-30940. APM acknowledge support from the NWO/DOME/IBM programme “Big Bang Big Data: Innovating ICT as a Driver For Astronomy”, project #628.002.001. We would like to thank the anonymous referee for useful comments that help to improve the presentation of our work.

Facilities: LOFAR, XMM-Newton, JVLA

REFERENCES

- Bonafede, A., Brügggen, M., Rafferty, D., et al. 2018, MNRAS, 478, 2927
- Bonafede, A., Brügggen, M., van Weeren, R., et al. 2012, MNRAS, 426, 40
- Bonafede, A., Feretti, L., Giovannini, G., et al. 2009, A&A, 503, 707
- Botteon, A., Shimwell, T. W., Bonafede, A., et al. 2019, A&A, 622, A19
- Botteon, A., Shimwell, T. W., Bonafede, A., et al. 2018, MNRAS, 478, 885
- Brunetti, G., & Jones, T. W. 2014, International Journal of Modern Physics D, 23, 1430007-98
- Brunetti, G., Giacintucci, S., Cassano, R., et al. 2008, Nature, 455, 944
- Brunetti, G. 2004, Journal of Korean Astronomical Society, 37, 493
- Cassano, R., Ettori, S., Brunetti, G., et al. 2013, ApJ, 777, 141

- Cassano, R., Brunetti, G., Norris, R. P., et al. 2012, *A&A*, 548, A100
- Cassano, R., Brunetti, G., Röttgering, H. J. A., & Brügger, M. 2010, *A&A*, 509, A68
- Cassano, R., Brunetti, G., & Setti, G. 2006, *MNRAS*, 369, 1577
- Cassano, R., & Brunetti, G. 2005, *MNRAS*, 357, 1313
- Cuciti, V., Cassano, R., Brunetti, G., et al. 2015, *A&A*, 580, A97
- de Gasperin, F., Dijkema, T. J., Drabent, A., et al. 2019, *A&A*, 622, A5
- Di Gennaro, G., van Weeren, R. J., Hoeft, M., et al. 2018, *ApJ*, 865, 24
- Dolag, K., Grasso, D., Springel, V., & Tkachev, I. 2005, *JCAP*, 1, 009
- Donnert, J., Vazza, F., Brügger, M., & ZuHone, J. 2018, *Space Sci. Rev.*, 214, 122
- Giovannini, G., & Feretti, L. 2000, *New Astronomy*, 5, 335
- Heymans, C., Van Waerbeke, L., Miller, L., et al. 2012, *MNRAS*, 427, 146
- Hoang, D. N., Shimwell, T. W., van Weeren, R. J., et al. 2019a, *A&A*, 622, A20
- Hoang, D. N., Shimwell, T. W., van Weeren, R. J., et al. 2019b, *A&A*, 622, A21
- Hoang, D. N., Shimwell, T. W., van Weeren, R. J., et al. 2018, *MNRAS*, 478, 2218
- Kale, R., Venturi, T., Giacintucci, S., et al. 2015, *A&A*, 579, A92
- Lindner, R. R., Baker, A. J., Hughes, J. P., et al. 2014, *ApJ*, 786, 49
- Mao, Y.-Y., Zentner, A. R., & Wechsler, R. H. 2018, *MNRAS*, 474, 5143
- McMullin J. P., Waters B., Schiebel D., Young W. & Golap K. 2007, in *Astronomical Society of the Pacific Conference Series*, Vol. 376, *Astronomical Data Analysis Software and Systems XVI*, ed. R. A. Shaw, F. Hill, & D. J. Bell, 127
- Mechev, A. P., Plaat, A., Oonk, J. B. R., Intema, H. T., & Röttgering, H. J. A. 2018, *Astronomy and Computing*, 24, 117
- Offringa, A. R., McKinley, B., Hurley-Walker, N., et al. 2014, *MNRAS*, 444, 606.
- Planck Collaboration, Ade, P. A. R., Aghanim, N., et al. 2016, *A&A*, 594, A27
- Sereno, M., Giocoli, C., Izzo, L., et al. 2018, *Nature Astronomy*, 2, 744
- Sereno, M., Covone, G., Izzo, L., et al. 2017, *MNRAS*, 472, 1946
- Shimwell, T. W., Luckin, J., Brügger, M., et al. 2016, *MNRAS*, 459, 277
- Shimwell, T. W., Röttgering, H. J. A., Best, P. N., et al. 2017, *A&A*, 598, A104
- Shimwell, T. W., Tasse, C., Hardcastle, M. J., et al. 2019, *A&A*, 622, A1
- Smirnov, O. M., & Tasse, C. 2015, *MNRAS*, 449, 2668
- Tasse, C., Hugo, B., Mirmont, M., et al. 2018, *A&A*, 611, A87
- Tasse, C. 2014a, *A&A*, 566, A127
- Tasse, C. 2014b, arXiv:1410.8706
- van Haarlem, M. P., Wise, M. W., Gunst, A. W., et al. 2013, *A&A*, 556, A2
- van Weeren, R. J., de Gasperin, F., Akamatsu, H., et al. 2019, *Space Sci. Rev.*, 215, 16
- van Weeren, R. J., Brunetti, G., Brügger, M., et al. 2016a, *ApJ*, 818, 204
- van Weeren, R. J., Williams, W. L., Hardcastle, M. J., et al. 2016b, *ApJS*, 223, 2
- van Weeren, R. J., Intema, H. T., Lal, D. V., et al. 2014, *ApJ*, 781, L32
- van Weeren, R. J., Röttgering, H. J. A., Brügger, M., & Cohen, A. 2009, *A&A*, 505, 991
- Vazza, F., Brunetti, G., Brügger, M., & Bonafede, A. 2018, *MNRAS*, 474, 1672
- Venturi, T., Giacintucci, S., Brunetti, G., et al. 2007, *A&A*, 463, 937
- Venturi, T., Giacintucci, S., Dallacasa, D., et al. 2008, *A&A*, 484, 327
- Wilber, A., Brügger, M., Bonafede, A., et al. 2019, *A&A*, 622, A25
- Wilber, A., Brügger, M., Bonafede, A., et al. 2018, *MNRAS*, 473, 3536
- Williams, W. L., van Weeren, R. J., Röttgering, H. J. A., et al. 2016, *MNRAS*, 460, 2385